Attenuation Correction for Cardiac Dual-Head γ Camera Coincidence Imaging Using Segmented Myocardial Perfusion SPECT

Kazuki Fukuchi, Masayoshi Sago, Koichi Nitta, Kazuhito Fukushima, Masahiro Toba, Kohei Hayashida, Makoto Takamiya, and Yoshio Ishida

Department of Radiology, National Cardiovascular Center, Suita, Osaka; and Bio-Medical Division, Sumitomo Metal Industries, Ltd., Tokyo, Japan

The diagnostic accuracy of cardiac FDG imaging obtained with the dual-head coincidence γ camera (DHC) is impaired by artifacts induced by nonuniform attenuation. This study proposed a new method (registration and segmentation method for attenuation correction [AC-RS]) to correct these attenuations in the chest region without the need for additional hardware or expensive transmission scanning equipment. **Methods:** Before DHC imaging, ^{99m}Tc-tetrofosmin SPECT was performed using dual-energy acquisition from both the photopeak and Compton scatter windows. The scatter window images of the ^{99m}Tc-tetrofosmin were then registered 3-dimensionally with the cardiac DHC images and segmented into anatomic regions to obtain body and lung contours by applying the optimal threshold method on localized histograms. Theoretic attenuation coefficient values were assigned to the corresponding anatomic regions, and the DHC emission images were reconstructed using these attenuation correction factors. The results were quantitatively evaluated by imaging a cardiac phantom filled with a uniform solution and placed in a chest phantom. Eight nondiabetic subjects were also examined using this technique, and the results were compared with those of measured attenuation-corrected PET images. **Results:** Use of this technique in phantom and clinical studies decreased the degree of artifacts seen in the inferior wall activity and corrected the emission images. When the results were compared with those of PET scans, the regional relative counts of the uncorrected DHC scan did not correlate with the results of the PET scan. However, the regional relative counts of the AC-RS–corrected DHC scan exhibited a linear correlation with the results of the PET scan ($r = 0.73$; $P < 0.001$). **Conclusion:** Reasonably accurate attenuation-corrected cardiac DHC images can be obtained using AC-RS without the need for transmission scanning.

Key Words: FDG; coincidence γ camera imaging; PET; attenuation correction

J Nucl Med 2000; 41:919–925

The use of γ cameras for FDG imaging has recently elicited considerable interest (*1–4*). FDG imaging can be performed using either a conventional SPECT system equipped with an ultra-high-energy collimator for 511-keV photons or a dual-head coincidence γ camera (DHC). In spite of the limited spatial resolution and sensitivity, the clinical feasibility of using FDG SPECT with an ultra-high-energy collimator for cardiac imaging has been investigated (*3,5–8*). On the other hand, attenuation artifacts can adversely affect the quality of cardiac DHC imaging (*3,4*). To apply DHC imaging to cardiac studies, an additional external transmission scan to correct attenuations is usually needed. However, external transmission scans require expensive hardware and software that are not included in a conventional DHC system (*9–11*).

The purpose of this preliminary study was to establish a method for correcting attenuations in cardiac DHC imaging if transmission imaging cannot be used. As an alternative to transmission imaging, a patient-specific attenuation map was obtained using ^{99m}Tc-tetrofosmin SPECT performed on the same day as the DHC imaging. We refer to this approach as the registration and segmentation method for attenuation correction (AC-RS). The method has been tested in phantoms and clinical studies.

MATERIALS AND METHODS

A schematic outline of the AC-RS technique is presented in Figure 1. ^{99m}Tc-tetrofosmin SPECT was performed using dual-energy acquisition from both the photopeak and the scatter windows. The cardiac DHC and the ^{99m}Tc-tetrofosmin images were registered 3-dimensionally, and the scatter window ^{99m}Tc-tetrofosmin images were segmented into several anatomic regions to visualize the body and lung contours by applying the optimal threshold method to localized histograms. The DHC emission images were then reconstructed using the theoretic values of the attenuation coefficients for each corresponding anatomic region.

Imaging Protocol

Patients were injected with 592 MBq ^{99m}Tc-tetrofosmin while at rest after having fasted overnight. Dual-peak window acquisition was performed using a dual-head SPECT system (Vertex-plus MCD; ADAC Laboratories, Milpitas, CA) equipped with a low-energy, high-resolution, parallel-hole collimator. Thirty-two projections (40 s/projection over 360° [180° × 2] in a 128 × 128 matrix)

Received May 3, 1999; revision accepted Sep. 14, 1999.

For correspondence or reprints contact: Yoshio Ishida, MD, PhD, Department of Radiology, National Cardiovascular Center, Fujishiro-dai 5-7-1, Suita, Osaka 565-8565 Japan.

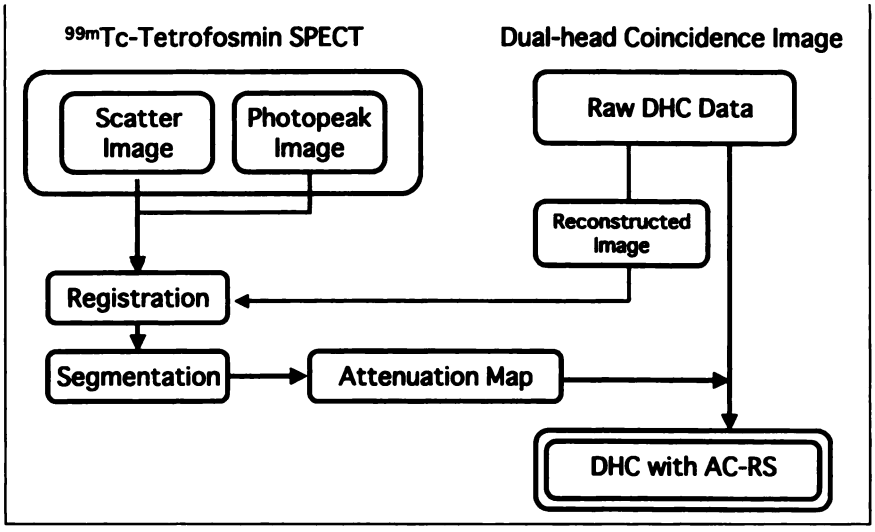

FIGURE 1. Block diagram illustrating various processing steps involved in AC-RS.

were obtained from the photopeak (141 keV ± 10%) and from the scatter (108 keV ± 10%) energy windows. Both sets of projections were reconstructed using 12 maximum-likelihood expectation-maximization iterations and Butterworth filtering (photopeak image, cutoff of 0.35 cycle/cm and order of 12; scatter window image, cutoff of 0.15 cycle/cm and order of 10).

After completion of the ^{99m}Tc-tetrofosmin image, 150 MBq FDG were injected 30 min after an oral glucose load. After an interval for decay of myocardial radioactivity, the DHC imaging was performed 160–180 min after the FDG injection. Sixty-four projections were obtained (30 s/projection every 5.6° over 360° [180° × 2] in a 128 × 128 matrix). The images were then reconstructed using ordered-subsets expectation-maximization iterative reconstruction. The DHC imaging was performed using the same camera system as that used for the ^{99m}Tc-tetrofosmin SPECT. A stationary laser system was used to ensure that the camera was roughly in the same position during both the ^{99m}Tc-tetrofosmin SPECT and the DHC imaging.

The dual-peak window ^{99m}Tc-tetrofosmin SPECT and the FDG-DHC imaging can be performed on the same day because injections of ^{99m}Tc-tetrofosmin do not interfere with FDG coincidence detection.

Registration

The images must be registered to produce an attenuation map from the ^{99m}Tc-tetrofosmin SPECT scatter window images because the ^{99m}Tc-tetrofosmin SPECT images and the DHC images were acquired at different times. We used a modified version of a previously described registration technique (*12,13*). The 3 reconstructed datasets for the DHC images, the scatter window images, and the photopeak images were entered into a computer and displayed. The DHC image was used as the reference, and the photopeak ^{99m}Tc-tetrofosmin SPECT image was registered accordingly. The photopeak and the scatter window data were acquired simultaneously, so their position was thus identical. The photopeak ^{99m}Tc-tetrofosmin SPECT image was resliced using the initial estimates of the x, y, and z translations and the transaxial, coronal, and sagittal rotations. The resliced photopeak ^{99m}Tc-tetrofosmin SPECT images were then visually compared with those of the DHC study. To determine the correspondence of anatomic landmarks rather than external markers, an elliptic or square region of interest (ROI) was placed adjacent to the heart in the DHC image. An ROI in the same position was then transferred to the photopeak ^{99m}Tc-tetrofosmin SPECT image. The photopeak ^{99m}Tc-tetrofosmin SPECT images were then registered with the DHC image by reference to the tracer uptake in the patient's heart and the ROI. After the 2 images were registered with very minimal discordance, the display was updated and the process was iterated. The registered scatter window image set was then saved on a hard disk.

Definition of Body Outline and Lung Boundaries

The segmentation strategy used in this study is a modification of a previously described method (*14,15*). First, the registered scatter window slices were used to segment the outline of the body. The second directional derivative in the direction of the count gradient was computed as a guide to estimate the position of the body outline. The derivative calculation is sensitive to both the noise in the image and the high uptake of radioactivity in the myocardium, which may cause a portion of the myocardial outline to be erroneously included in the outline of the body. To prevent this result, the image was reconstructed using the maximum-likelihood expectation-maximization algorithm to decrease the noise from scatter photons in the myocardium, and an interactive threshold program was used to assist in the estimation of the body outline. A threshold was selected that allowed the degree of external radioactivity to be distinguished from the degree of internal radioactivity. After the outline of the body had been determined, a counts-threshold–based segmentation program was used to segment the regions of the lungs.

Calculation of Attenuation Coefficient Factors

Once the regions were segmented, theoretic values at 511-keV based on previously published estimates were assigned to the pixels of each segmented region (soft tissue, 0.095/cm; lung, 0.035/cm) (*16,17*). The chest attenuation map consisted primarily of regions of soft tissue (water) and lung. The spine and the other bones of the thorax were indistinguishable from the soft tissue in the scatter window images, because their theoretic attenuation coefficient was almost identical to that of water (*18*). After the attenuation coefficient values had been assigned, the new attenuation values for each pixel in the image were forward projected onto the sinograms of the DHC image and then used to correct the attenuation in the emission sinograms. Each processing step was

completed using a Pegasys computer system (ADAC) and an Ultra workstation (SUN Microsystems, Inc., Palo Alto, CA).

Phantom Study

An anthropomorphic thorax phantom was used to validate the accuracy of the AC-RS method. To produce an attenuation map, the lung compartments were filled with damp Styrofoam beads (The Dow Chemical Company, Midland, MI), the heart compartment was filled with a solution of 5.2 MBq ^{99m}Tc pertechnetate, and the remainder of the phantom was filled with a solution of 37 MBq ^{99m}Tc pertechnetate to represent the soft-tissue background. The concentration of activity in the liver was 11.1 kBq/mL, and the activity in the mediastinum was approximately half that in the liver. DHC imaging was performed using the same phantom, but the heart compartment was filled with a solution of 10 MBq FDG.

The imaging protocol and the image reconstruction were as described above. Bull's-eye polar maps were prepared before and after the AC-RS and then compared to assess the uniformity of counts in the cardiac walls.

Clinical Study

Eight patients who were referred to our department for cardiac FDG studies between October 1998 and April 1999 (3 women, 5 men; age range, 56–75 y; mean age [±SD], 64.8 ± 6.8 y) were included in this study. None of the patients were diabetic. All of the patients had undergone coronary angiography and left ventriculography within 2 weeks of a radionuclide study. Significant coronary stenosis was defined as a ≥75% reduction in the luminal diameter of at least 1 major epicardial coronary artery, as determined by coronary angiography. The average left ventricular ejection fraction of the patients was 45.5% ± 14.9%. Four of the patients exhibited coronary artery disease, as shown by angiography, and had a history of myocardial infarction. A myocardial perfusion defect was seen on ^{99m}Tc-tetrofosmin SPECT for all 4 of these patients, confirming the presence of a significant stenosis and a regional left ventricular wall motion abnormality. Three other patients with coronary artery disease exhibited significant coronary stenosis, but their myocardial perfusions were normal at rest. The last patient exhibited mitral regurgitation but showed no sign of significant coronary stenosis. Our protocol was approved by the institutional review board, and all patients gave their written informed consent.

Transmission-corrected PET was also performed to obtain a standard cardiac FDG distribution using a SET 1400W system (Shimadzu Co., Kyoto, Japan). Transmission scanning was performed for 8 min using a ^{68}Ge–^{68}Ga line source. Twelve minutes of emission data were obtained 40 min after the FDG injection, and the image was consecutively reconstructed using the measured attenuation coefficients based on the transmission data. Images were reconstructed by filtered backprojection on a 128 × 128 matrix using a Butterworth filter.

To compare the regional cardiac FDG distributions in all 3 imaging procedures (DHC imaging with and without AC-RS, and PET), the data for each patient were analyzed using the 16-ROI method. The 2 image slices of the distal and basal short axial images were divided into 8 segments. The uptake of FDG in each segment was then quantified as the percentage of the average uptake in each ROI compared with the maximal FDG uptake.

Statistical Analysis

Linear regression analysis was performed to calculate the linear dependency of the regional FDG uptake in each anatomic region for each imaging procedure. A probability level of less than 0.05 was considered to indicate a significant difference.

RESULTS

Phantom Study

The results of the phantom studies are shown in Figure 2. Figure 3 shows the standard views and the bull's-eye display produced by the phantom studies. The count density of the inferior wall was reduced by approximately 75% when the studies were reconstructed without attenuation correction. When AC-RS was used, however, the attenuation artifact was eliminated, and the variation in the mean count density was less than that of the uncorrected data.

Clinical Study

ROIs were defined in regions of lung and soft tissues (mediastinum and chest wall) on PET transmission scans for each patient. The mean count per pixel in each ROI was measured, and the ratio of the soft-tissue count to that of the lung-tissue count (S/L) was calculated. The S/L of the measured transmission data was 2.66, which is similar to the ratio in the assumed attenuation coefficient (2.71) for soft tissue and lung tissue.

Representative images of the scatter window of the ^{99m}Tc-tetrofosmin image and the segmented attenuation map are shown in Figure 4. The body and lung boundaries were clearly outlined using the data from the scatter window images of each patient. Myocardial DHC images of the patients were reconstructed with and without the AC-RS method. An example of the image obtained in a patient with no history of myocardial infarction using this protocol is shown in Figure 5.

Quantitative data for images obtained with and without AC-RS correction were compared with those of PET images in 16 regions of the heart. Because the effects of attenuation correction vary from region to region, the effects of AC-RS were assessed in 2 different myocardial regions: the inferior-to-septal region, where attenuation artifacts are most likely to occur, and the anterior-to-lateral region. Without attenuation correction, the values of both regions were different from those of the PET image. The relative uptake in the DHC image was higher than that in the PET image in the anterior-to-lateral region, whereas the DHC uptake was lower than that of the PET image in the inferior-to-septal region. The relative uptake of DHC without attenuation correction did not correlate with the data from the PET studies (Fig. 6A). With AC-RS, on the other hand, the relative regional uptake seen in the DHC images corrected well with the uptake value seen in the PET images for both inferior-to-septal and anterior-to-lateral regions (Fig. 6B). A linear fit was found between the quantitative values for the DHC images with AC-RS and the attenuation-corrected PET images ($r = 0.73$; $P < 0.001$).

DISCUSSION

This study shows that the AC-RS method can be used to obtain attenuation maps from scatter window ^{99m}Tc images.

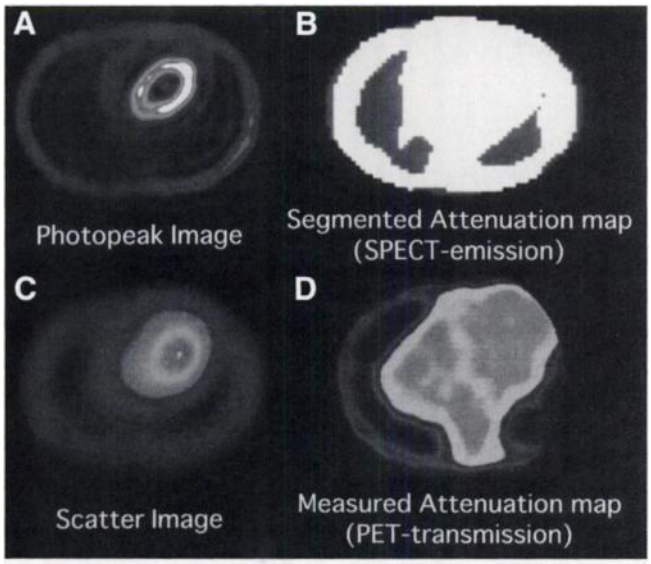

FIGURE 2. Transaxial phantom images of photopeak (A) and Compton scatter data (C) with ^{99m}Tc-tetrofosmin SPECT. In C, chest wall and lung boundaries are clearly visualized. Segmented attenuation map (B), generated using scatter image, is comparable with measured attenuation map (D), derived from PET transmission imaging.

These maps can then be used to correct attenuation artifacts in the DHC images if the tissue attenuation is assumed to be uniform within the lung and body tissues. In our protocol, a myocardial SPECT scan using ^{99m}Tc-tetrofosmin was used to correct DHC images. The additional administration of radionuclides that is required by this procedure results in a modest increase in the dose absorbed by the patients. Although our approach results in a somewhat higher radiation burden than that delivered in transmission studies, the information that can be obtained from a ^{99m}Tc-tetrofosmin SPECT scan is often necessary to evaluate the myocardial perfusion of patients. Thus, this technique is recommended for use as part of a study that combines FDG DHC and perfusion SPECT.

Attenuation Artifacts in DHC Imaging

Our data indicate that cardiac DHC imaging is usually affected by image artifacts, resulting in an FDG uptake value different from that obtained using an attenuation-corrected PET scan. This result is similar to that described in previous papers (*3,4*). Image artifacts occur because 2 γ rays are emitted from the body in opposite directions during positron imaging. Thus, photons must exit the body in 2 locations. As a result of these attenuation artifacts, cardiac DHC imaging has not been enthusiastically promoted regardless of its physical performance advantages over FDG SPECT systems equipped with an ultra-high-energy (511-keV) collimator (*4,19*).

This study showed that DHC without attenuation correction displays regional counts that are as much as 60% lower than attenuation-corrected PET values. These figures are critical in assessing myocardial viability, because 50% of the maximum activity is usually considered to be the threshold for reliable distinctions between viable and nonviable tissue in FDG PET (*20*). Thus, the DHC images without attenuation correction may not be useful for determining myocardial viability, although FDG SPECT scans using an ultra-high-energy collimator have enjoyed some success in this area (*3,5–8*).

Impact of Attenuation Correction

Several methods have been proposed to correct attenuation in myocardial SPECT scans, because the quality of the tracer in the septal and inferoposterior regions of the myocardium can be as much as 30%–50% lower than that in the anterior region as a result of attenuation (*17*). In most of these methods, the distribution of the attenuation coefficients in the chest must be determined. These attenuation coefficients are usually determined by transmission measurements

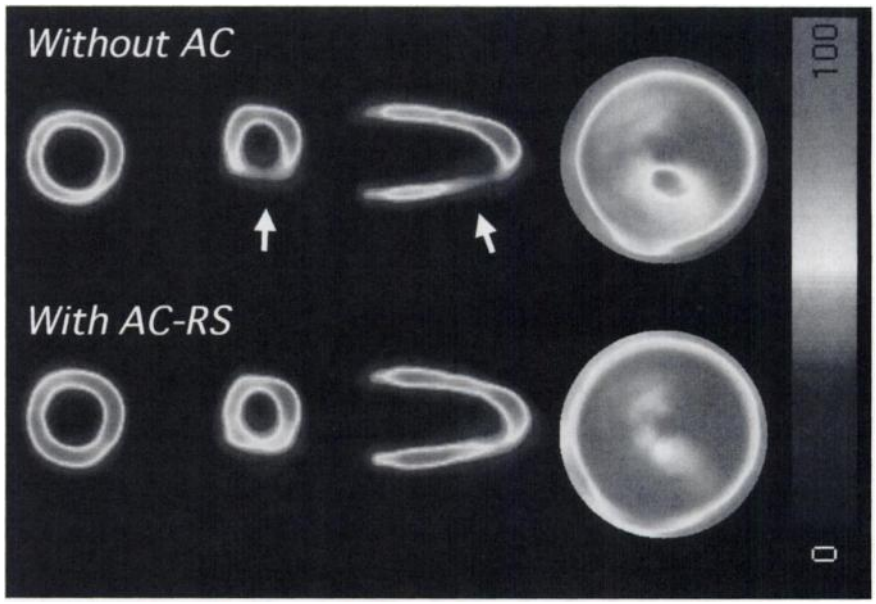

FIGURE 3. Representative images of 2 orthogonal views and bull's-eye map obtained from DHC images without attenuation correction (AC) (top) and with AC-RS (bottom).

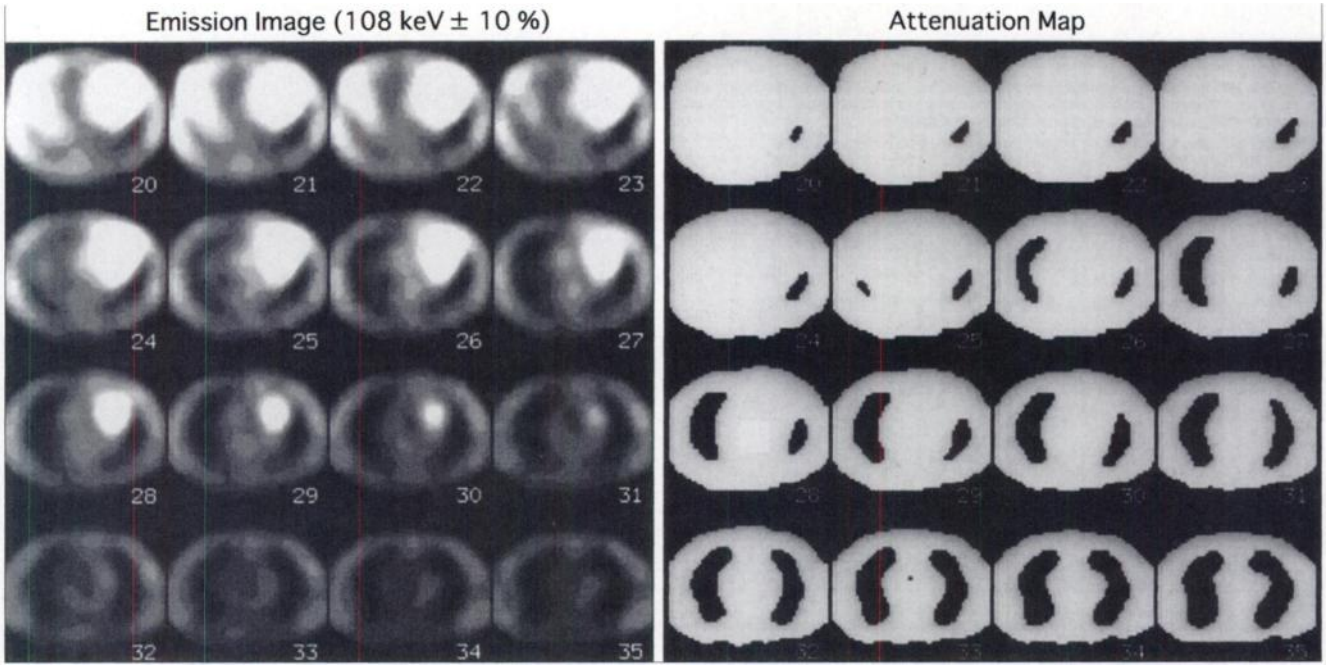

FIGURE 4. Representative clinical study showing Compton scatter data of dual-peak window ^{99m}Tc-tetrofosmin SPECT image and segmented attenuation map.

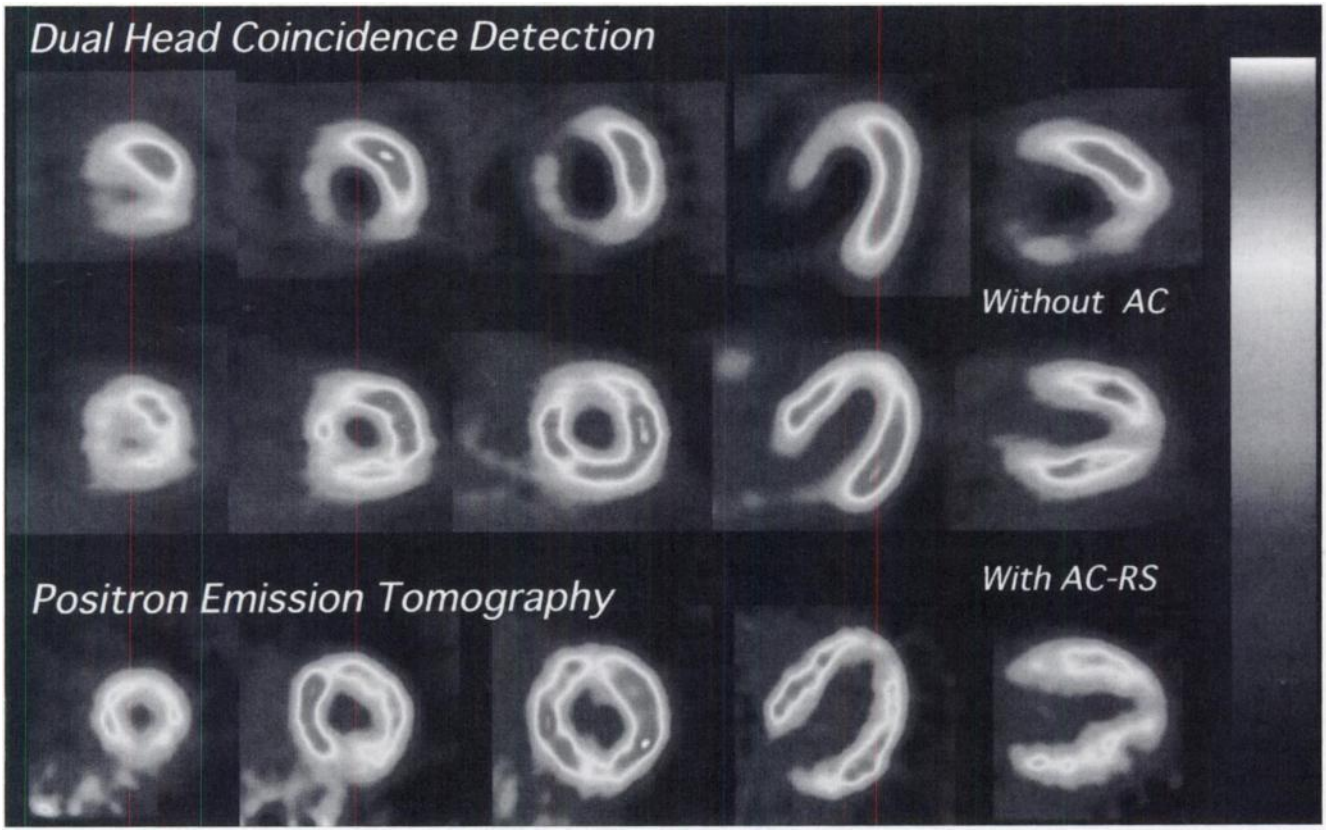

FIGURE 5. Myocardial FDG images from 44-y-old man with no history of myocardial infarction. Without attenuation correction (AC), attenuation effects were noted in inferior and inferior-to-septal regions of myocardium. With AC-RS, however, images of myocardium are nearly uniform and are similar to attenuation-corrected PET images.

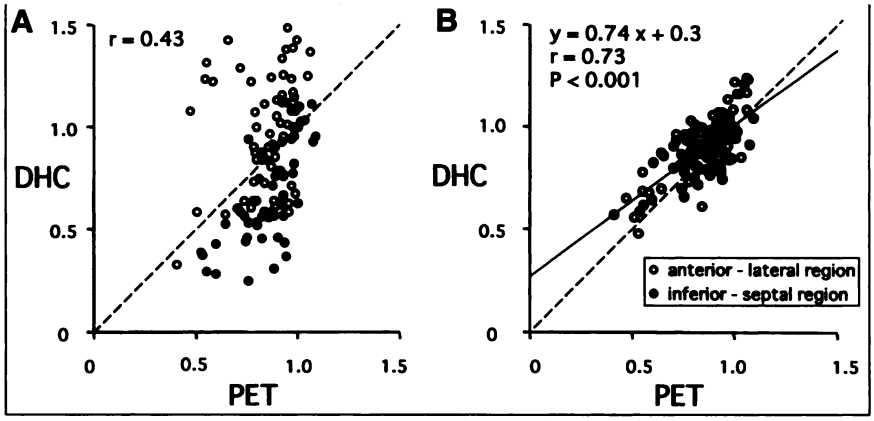

FIGURE 6. Comparison of relative FDG uptake values obtained using PET and those obtained using DHC without attenuation correction (A) and with AC-RS (B).

(*21–23*). Although these methods are effective, the required equipment is awkward and expensive.

This study describes a new attenuation correction method for cardiac DHC imaging using segmented myocardial perfusion SPECT instead of transmission scanning. Although the steps after processing require a longer time, the use of segmented scatter window ^{99m}Tc-tetrofosmin SPECT images to estimate attenuation maps offers several advantages. First, this emission-based attenuation correction method does not require additional hardware. Consequently, institutions equipped with a DHC-capable camera can use this procedure for reliable imaging even if they do not possess the equipment required to generate a transmission image. The scatter window data are acquired simultaneously using the additional energy window in myocardial perfusion studies. Thus, our method can be adapted to clinical use with only minor changes to the present imaging protocol.

Our data indicate that the AC-RS method can be used to decrease the attenuation artifacts in the DHC imaging and improve the conformity of relative FDG counts in DHC and attenuation-corrected PET images. When 2 myocardial regions (i.e., the anterior-to-lateral region and the inferior-to-septal region) were examined separately, both regions showed a significant improvement with AC-RS. Thus, AC-RS appears to be capable of improving estimates of FDG uptake, in the inferior-to-septal region, where attenuation artifacts are most likely to occur, and in the anterior-to-lateral region. AC-RS appears to be a reliable attenuation correction method that can be used for quantitative purposes. The results also suggest the possibility of quantitative DHC studies using standard uptake values, which are commonly used in PET studies without the need for additional transmission scanning.

Limitations

One of the most difficult steps in the AC-RS method was the registration of the DHC images and the scatter window ^{99m}Tc-tetrofosmin images. These 2 images were acquired under very different conditions, including different photon energies, reconstruction parameters, and times of acquisition. To register the images accurately, the photopeak ^{99m}Tc-tetrofosmin images were used instead of the scatter window images. We also used ROIs as markers and 3-dimensional dataset fitting. This approach improved the matching accuracy and made the method more convenient. By displaying the 3 orthogonal views, we could easily detect even small displacements in any orientation. The disadvantages of this method include operator subjectivity and the time required to correct motion (3-dimensional linear and angular displacements). A fully automated methodology for registering ^{99m}Tc-tetrofosmin SPECT and DHC images would greatly improve the convenience of this method.

Another emission-based attenuation correction method using ^{99m}Tc-macroaggregated albumin (MAA) lung SPECT has been proposed (*24,25*). The lung boundaries in images produced using ^{99m}Tc-MAA lung perfusion scans are more accurate, but ^{99m}Tc-MAA scans do not provide any information that can contribute to a diagnosis of heart disease. Scatter images from myocardial perfusion scans, however, can be used to generate patient-specific attenuation maps and provide information on myocardial perfusion, which is the most important aspect of nuclear cardiology. In studies combining FDG DHC and perfusion SPECT, the AC-RS method may be more reliable than attenuation corrections using ^{99m}Tc-MAA lung scans.

In this study, attenuation correction was applied to only the DHC images; the ^{99m}Tc-tetrofosmin SPECT images were not corrected. Matsunari et al. (*26*) reported that uncorrected ^{99m}Tc-tetrofosmin SPECT images tend to underestimate the detection of myocardial viability and that attenuation correction increases the degree of conformity between ^{99m}Tc-tetrofosmin SPECT and FDG PET images. Theoretically, the AC-RS method can also be applied to ^{99m}Tc-tetrofosmin SPECT images because this form of emission-based attenuation correction was originally developed for ^{99m}Tc-labeled myocardial SPECT scans (*14,15*). More sophisticated studies using FDG DHC and perfusion SPECT will be performed by applying AC-RS to both DHC and ^{99m}Tc-tetrofosmin SPECT images.

CONCLUSION

This study shows that reasonably accurate attenuation-corrected cardiac DHC images can be obtained using

registered and segmented myocardial perfusion SPECT images. This method improves nonuniform attenuation artifacts in DHC imaging without the use of a transmission scan and can be applied to situations in which transmission images cannot be produced.

ACKNOWLEDGMENTS

The authors thank Yoshinori Miyake for technical support in the production of FDG and Nobuyoshi Kita, Hisashi Oka, Tetsuro Katafuchi, and Takao Nishihara for skilled technical support in the imaging studies.

REFERENCES

1. Conti PS, Keppler JS, Halls JM. Positron emission tomography: a financial and operational analysis. *AJR.* 1994;162:1279–1286.
2. Jarritt PH, Acton PD. PET imaging using gamma camera systems: a review. *Nucl Med Commun.* 1996;17:758–766.
3. Sandler MP, Bax JJ, Patton JA, Visser FC, Martin WH, Wijns W. Fluorine-18-fluorodeoxyglucose cardiac imaging using a modified scintillation camera. *J Nucl Med.* 1998;39:2035–2043.
4. Patton JA, Turkington TG. Coincidence imaging with a dual-head scintillation camera. *J Nucl Med.* 1999;40:432–441.
5. Martin WH, Delbeke D, Patton JA, et al. FDG-SPECT: correlation with FDG-PET. *J Nucl Med.* 1995;36:988–995.
6. Chen EQ, MacIntyre WJ, Go RT, et al. Myocardial viability studies using fluorine-18-FDG SPECT: a comparison with fluorine-18-FDG PET. *J Nucl Med.* 1997;38:582–586.
7. Bax JJ, Cornel JH, Visser FC, et al. Prediction of improvement of contractile function in patients with ischemic ventricular dysfunction after revascularization by fluorine-18 fluorodeoxyglucose single-photon emission computed tomography. *J Am Coll Cardiol.* 1997;30:377–383.
8. Srinivasan G, Kitsiou A, Bacharach S, Bartlett M, Miller-Davis C, Dilsizian V. [^{18}F]fluorodeoxyglucose single photon emission computed tomography: can it replace PET and thallium SPECT for the assessment of myocardial viability? *Circulation.* 1998;97:843–850.
9. Halama JR, Henkin RE, Krzos JR. Improved image quality and lesion detection in gamma camera coincidence imaging of positron emitters with measured attenuation correction [abstract]. *J Nucl Med.* 1998;39(suppl):38P.
10. Laymon CM, Turkington TG, Gilland DR, Coleman RE. Transmission scanning on a gamma camera coincidence imaging system [abstract]. *J Nucl Med.* 1998;39(suppl):92P.
11. Shao L, Nellemann P, Muehllehner G, Bertelsen H, Hines H. Singles-transmission attenuation correction for dual head coincidence imaging [abstract]. *J Nucl Med.* 1998;39(suppl):37P.
12. Pietrzyk U, Herholz K, Fink G, et al. An interactive technique for three-dimensional image registration: validation for PET, SPECT, MRI and CT brain studies. *J Nucl Med.* 1994:35;2011–2018.
13. Pietrzyk U, Herholz K, Heiss WD. Three-dimensional alignment of functional and morphological tomograms. *J Comput Assist Tomogr.* 1990;14:51–59.
14. Pan TS, King MA, Luo DS, Dahlberg ST, Villegas BJ. Estimation of attenuation maps from scatter and photopeak window single photon-emission computed tomographic images of technetium 99m-labeled sestamibi. *J Nucl Cardiol.* 1997;4:42–51.
15. Pan TS, King MA, de Vries DJ, Ljungberg M. Segmentation of the body and lungs from Compton scatter and photopeak window data in SPECT: a Monte-Carlo investigation. *IEEE Trans Med Imaging.* 1996;15:13–24.
16. Xu M, Luk WK, Cutler PD, Digby WM. Local threshold for segmented attenuation correction of PET imaging of the thorax. *IEEE Trans Nucl Sci.* 1994;41:1532–1537.
17. Sorenson JA, Phelps ME. *Physics in Nuclear Medicine.* 2nd ed. Philadelphia, PA: WB Saunders; 1987.
18. Xu EZ, Mullani NA, Gould KL, Anderson WL. A segmented attenuation correction for PET. *J Nucl Med.* 1991;32:161–165.
19. Shreve P, Steventon R, Deters E, Kison P, Gross M, Wahl R. Oncologic diagnosis with 2-[fluorine-18]fluoro-2-deoxy-D-glucose imaging: dual-head coincidence gamma camera versus positron emission tomographic scanner. *Radiology.* 1998; 207:431–437.
20. Baer FM, Voth E, Deutsch HJ, Schneider CA, Schicha H, Sechtem U. Assessment of viable myocardium by dobutamine transesophageal echocardiography and comparison with fluorine-18 fluorodeoxyglucose positron emission tomography. *J Am Coll Cardiol.* 1994;24:343–353.
21. Kluge R, Sattler B, Seese A, Knapp WH. Attenuation correction by simultaneous emission-transmission myocardial single-photon emission tomography using a technetium-99m-labelled radiotracer: impact on diagnostic accuracy *Eur J Nucl Med.* 1997;24:1107–1114.
22. He ZX, Scarlett MD, Mahmarian JJ, Verani MS. Enhanced accuracy of defect detection by myocardial single-photon emission computed tomography with attenuation correction with gadolinium 153 line sources: evaluation with a cardiac phantom. *J Nucl Cardiol.* 1997;4:202–210.
23. Prvulovich EM, Lonn AH, Bomanji JB, Jarritt PH, Ell PJ. Effect of attenuation correction on myocardial thallium-201 distribution in patients with a low likelihood of coronary artery disease. *Eur J Nucl Med.* 1997;24:266–275.
24. Wallis JW, Miller TR, Koppel P. Attenuation correction in cardiac SPECT without a transmission measurement. *J Nucl Med.* 1995;36:506–512.
25. Madsen MT, Kirchner PT, Grover-MacKay M, et al. Emission-based attenuation correction of myocardial perfusion studies. *J Nucl Cardiol.* 1997;4:477–486.
26. Matsunari I, Boning G, Ziegler SI, et al. Attenuation-corrected ^{99m}Tc-tetrofosmin single-photon emission computed tomography in the detection of viable myocardium: comparison with positron emission tomography using ^{18}F-fluorodeoxyglucose. *J Am Coll Cardiol.* 1998;32:927–935.